

# Temperature Equilibration Rate of Quasi-Monoenergetic Deuteron Beam in a Fusion Plasmas

M. Mahdavi<sup>1\*</sup> R. Azadifar<sup>1†</sup> and T. Koorokhi<sup>2‡</sup>

<sup>1</sup>Physics Department, University of Mazandaran, P. O. Box 47415-416, Babolsar, Iran

<sup>2</sup>Physics Department, Faculty of Sciences, Golestan University, Shahid Beheshti Street, P.O.  
Box 155, Gorgan, Iran

---

\*email: m.mahdavi@umz.ac.ir

†email: r.azadifarr@gmail.com

‡email: t.koohrokhi@gu.ac.ir

## Abstract

Thermal equilibrium rate can play an important role in the energy deposition of beam to the fuel in fast ignition due to high temperature difference between projectile ions and background plasma ions. In this study the temperature equilibration rate of a quasi-monoenergetic deuteron beam with an equimolar Deuterium-Tritium fusion plasma with a Maxwellian energy distribution is calculated by kinetic theory equations. In this theory, binary collisions is described by the Boltzman equation and collective effects is described by the Lenard-Balescu equation. The obtained results show that at higher background temperatures,  $T_b = 100keV$ , the ions interactions effect in the temperature equilibration rate increases because the deuteron beam exchanges most of its energy with ions plasma.

**Key words:** Deuteron Beam; Temperature Equilibration Rate; Binary Collisions; Collective interactions.

# 1 Introduction

A typical plasma which is formed at ignition and burn stages of an inertial confinement fusion fuel is known as a hot dense plasma [1]. The plasma temperature ( $T \simeq 10\text{-}100$  keV) exceeds the sun's temperature during burning and the capsule is compressed to high densities ( $\rho \simeq 300 - 500 \text{ gcm}^{-3}$ ) at the ignition instance [2]. The determinative conditions of a plasma are determined by its temperature and density, spontaneously [3]. Despite of high temperature and density, the fusion plasma in the inertial confinement fuel capsule is a weakly coupled plasma [4]. A non-interacting weakly coupled plasma is described by Maxwell-Boltzmann distribution function at the thermal equilibrium [5]. Nevertheless, a fusion plasma is an interacting plasma whose temperature of plasma species (different ions and electrons) is changed by the energy gain and loss mechanisms. For different characteristic properties of particles (mass, charge etc), the plasma species have different temperatures during burning of fuel. The particles with different temperatures exchange their energy together via collisions and collective interactions [6]. The dynamical analyses of the igniting and burning of fusion plasma require exact calculations for temperature equilibration rate of plasma species.

The plasma kinetic theory is derived from statistical mechanics and describes the evolution of particles distribution functions [7]. In the plasma kinetic theory, the Boltzmann equation for Coulomb and nuclear elastic scattering describes the short-distance, hard collisions of the plasma particles whereas the long-distance, collective excitations of the plasma, is described by the Lenard-Balescu equation [8,9]. This theory has been used for calculation of temperature equilibration rate of two particles with Maxwell-Boltzmann distribution functions at two different temperatures. On the other hand, ion fast ignition using quasi-monoenergetic ion beams as ignitor have been proposed and studied after production of laser accelerated quasi-monoenergetic ion beams, experimentally [10,11]. The

narrow energy spread and high conversion efficiency of quasi-monoenergetic laser-driven high-current ions, make them very suitable for local energy deposition. Among the ion beams which were studied as ignitor, the deuteron beam has special privilege, because the deuteron beam can experience fusion reactions during deposition of its energy via stopping into the fuel [12,13]. These reasons promoted us to study a quasi-monoenergetic deuteron beam as the projectile that deposits its energy into an equimolar deuterium-tritium plasma. The obtained results are remarkable and applicable for accurate simulations and advanced codes.

## 2 Projectile and Background Particles Distribution Functions

The distribution function of quasi-monoenergetic projectile beam has been considered as the Gaussian function as [14],

$$f_p(E_p) = \frac{n_p \sqrt{\alpha}}{\Delta \sqrt{\pi}} \exp \left[ -\alpha \left( \frac{E_p - E_0}{\Delta} \right)^2 \right]. \quad (1)$$

where  $n_p$  is number of densities of projectile ions and  $\alpha = 4\ln(2)$ . The  $E_0 = \langle E_p \rangle$  is the average kinetic energy of ions in which for quasi-monoenergetic distribution function is equal to projectile temperature  $T_p$ . The quantity  $\Delta = \Delta E/E$  is the energy spread so that high quality projectile beam has 10% [15]. If the energy spread  $\Delta$  (full width at half maximum, FWHM) is 10%, this distribution refer to as "quasi-monoenergetic". Corresponding the relation  $\int f_p(\mathbf{v}_p) d^3v_p = \int f_p(E_p) dE_p$  and projectile kinetic energy  $E_p = \frac{1}{2}m_p v_p^2$ , the quasi-monoenergetic velocity distribution in the phase space is,

$$f_p(\mathbf{v}_p) = \frac{2n_p(\pi\hbar^2)^{3/2}\sqrt{\alpha}}{\Delta m_p^2 v_p} \exp \left[ -\alpha \left( \frac{m_p v_p^2}{2\Delta} - \frac{E_0}{\Delta} \right)^2 \right]. \quad (2)$$

where  $m_p$  and  $v_p$  are the mass and velocity of projectile, respectively. In a fusion plasma, the velocity distribution function of background particles  $b$  at thermal equilibrium is considered as Maxwellian form,

$$f_b(\mathbf{v}_b) = n_b \left( \frac{2\pi\hbar^2\beta_b}{m_b} \right)^{3/2} \exp\left(-\frac{1}{2}\beta_b m_b v_b^2\right). \quad (3)$$

where  $\beta_b = 1/T_b$ ,  $m_b$ ,  $v_b$  and  $n_b$  are the inverse temperature, mass, velocity and number density of 'b' particle, respectively. For next purposes, we need multiply the two projectile and background distribution functions,

$$f_p(\mathbf{v}_p) f_b(\mathbf{v}_b) = \frac{n_p n_b 2^{5/2} (\pi\hbar^2)^3 \sqrt{\alpha}}{\Delta m_p^2 m_b^{3/2} v_p T_b^{3/2}} \exp\left[-\alpha \left( \frac{m_p v_p^2 T_p}{2\Delta} \frac{T_p}{\Delta} \right)^2 - \frac{1}{2}\beta_b m_b v_b^2\right]. \quad (4)$$

Furthermore, as we will see soon, it is useful to change laboratory velocities to the center of mass  $\mathbf{V}_c$  and relative  $\mathbf{v}_{pb} = \mathbf{v}_p - \mathbf{v}_b$  velocities as,

$$\begin{cases} \mathbf{v}_p = \mathbf{V}_c + \frac{m_b}{M_{pb}} \mathbf{v}_{pb} \Rightarrow v_p^2 = V_c^2 + \frac{m_b^2}{M_{pb}^2} v_{pb}^2 + 2\mathbf{V}_c \cdot \mathbf{v}_{pb} \frac{m_b}{M_{pb}} \\ \mathbf{v}_b = \mathbf{V}_c - \frac{m_p}{M_{pb}} \mathbf{v}_{pb} \Rightarrow v_b^2 = V_c^2 + \frac{m_p^2}{M_{pb}^2} v_{pb}^2 - 2\mathbf{V}_c \cdot \mathbf{v}_{pb} \frac{m_p}{M_{pb}}, \end{cases} \quad (5)$$

Replacing these translations into Eq. (4), leads,

$$\begin{aligned} f_p(\mathbf{v}_p) f_b(\mathbf{v}_b) &= \frac{n_p n_b 2^{5/2} (\pi\hbar^2)^3 \sqrt{\alpha}}{\Delta m_p^2 m_b^{3/2} v_p T_b^{3/2}} \left( V_c^2 + \frac{m_b^2}{M_{pb}^2} v_{pb}^2 + 2\mathbf{v}_{pb} \cdot \mathbf{V}_c \frac{m_b}{M_{pb}} \right)^{-1/2} \times \\ &\exp\left\{ -\frac{\alpha}{\Delta^2} \left[ \frac{m_p^2 V_c^4}{4} + \frac{m_{pb}^4 v_{pb}^4}{4m_p^2} + m_{pb}^2 (\mathbf{v}_{pb} \cdot \mathbf{V}_c)^2 - \left( m_p T_p - \frac{\Delta^2 m_b}{2\alpha T_b} - m_{pb} m_p \mathbf{v}_{pb} \cdot \mathbf{V}_c \right) V_c^2 \right. \right. \\ &\left. \left. - \left( \frac{T_p}{m_p} - \frac{\Delta^2}{2m_b \alpha T_b} - \frac{m_{pb}}{m_p} \mathbf{v}_{pb} \cdot \mathbf{V}_c - \frac{V_c^2}{2} \right) m_{pb}^2 v_{pb}^2 - \left( 2T_p + \frac{\Delta^2}{\alpha T_b} \right) m_{pb} \mathbf{v}_{pb} \cdot \mathbf{V}_c + T_p^2 \right] \right\} \quad (6) \end{aligned}$$

This relation will be used in the next sections.

### 3 The Energy Exchange Rate Due to Binary Collisions

The energy exchange rate between projectile ions and background particles of plasma due to binary collisions is evaluated by Boltzmann equation [16]:

$$\frac{d\varepsilon_{pb}}{dt} = \int \frac{d^3\mathbf{p}_b}{(2\pi\hbar)^3} \frac{d^3\mathbf{p}_p}{(2\pi\hbar)^3} f_b(\mathbf{p}_b) f_p(\mathbf{p}_p) v_{pb} \int d\Omega \left( \frac{d\sigma_{pb}}{d\Omega} \right) [E'_p - E_p], \quad (7)$$

where  $E_p$  and  $E'_p$  are the kinetic energies of projectile before and after one collision, respectively. Since in an elastic collision, Coulomb as well as nuclear potentials are contributed to the scattering, the total elastic scattering cross section ( $d\sigma_{pb}/d\Omega$ ) is the sum of Coulomb ( $d\sigma_{pb}^{\text{Coul}}/d\Omega$ ) and nuclear ( $d\sigma_{pb}^{\text{NI}}/d\Omega$ ) cross sections, [17]. The experimental data for these quantities are available in Ref. [18]. In the quantum mechanics, there are differences between the scattering of identical particles, such as deuterium-deuterium (D+D), and distinguishable particles such as deuterium-tritium (D+T). The Coulomb scattering is represented by the Rutherford formula for distinguishable particles [19],

$$\left( \frac{d\sigma}{d\Omega} \right)_{cd}^{\text{Coul}} = \frac{\eta^2}{k^2(1-\mu)^2}, \quad (8)$$

and for identical particles is presented as,

$$\left( \frac{d\sigma}{d\Omega} \right)_{ci}^{\text{Coul}} = \frac{2\eta^2}{k^2(1-\mu^2)} \left[ \frac{1+\mu^2}{1-\mu^2} + \frac{(-1)^{2s}}{2s+1} \cos \left( \eta \ln \frac{1+\mu}{1-\mu} \right) \right], \quad (9)$$

where  $s$  is the spin of identical particles,  $\mu = \cos\Theta$  is cosine of the scattering angle in the center-of-mass system,  $k$  is particle wave number and  $\eta$  is the dimensionless Coulomb parameter,

$$\eta_{pb} = \frac{Z_p Z_b e^2}{\hbar v_{pb}}, \quad (10)$$

The nuclear elastic scattering cross section for identical particles may be written as,

$$\left( \frac{d\sigma}{d\Omega} \right)_{ci}^{\text{NI}} = -\frac{2\eta}{1-\mu^2} \text{Re} \left\{ \sum_{\ell=0}^{NL} \left[ (1+\mu) \exp \left( i\eta \ln \frac{1-\mu}{2} \right) + (-1)^\ell (1-\mu) \right] \right\}$$

$$\times \exp\left(i\eta \ln \frac{1+\mu}{2}\right) \left] \frac{2\ell+1}{2} a_\ell(E) P_\ell(\mu) \right\} + \sum_{\ell=0}^{NL} \frac{4\ell+1}{2} b_\ell(E) P_{2\ell}(\mu), \quad (11)$$

and the nuclear cross section for distinguishable particles is,

$$\begin{aligned} \left(\frac{d\sigma}{d\Omega}\right)_{cd}^{\text{NI}} &= -\frac{2\eta}{1-\mu} \text{Re} \left\{ \exp\left(i\eta \ln \frac{1-\mu}{2}\right) \sum_{\ell=0}^{NL} \frac{2\ell+1}{2} a_\ell(E) P_\ell(\mu) \right\} \\ &+ \sum_{\ell=0}^{2NL} \frac{2\ell+1}{2} b_\ell(E) P_\ell(\mu), \end{aligned} \quad (12)$$

The value of NL represents the highest partial wave contributing to nuclear scattering.  $a_\ell$  are complex coefficients for expanding the trace of the nuclear scattering amplitude matrix and  $b_\ell$  coefficients are real coefficients for expanding the nuclear scattering cross section which are derived from experimental data.  $P_\ell(\mu)$  and  $P_{2\ell}(\mu)$  are also Legendre functions.

The change in projectile kinetic energy as a result of the collision is equal to [20],

$$E'_p - E_p = m_{pb} V_c v_{pb} \left( x(\mu - 1) + \sqrt{(1-x^2)(1-\mu^2)} \right), \quad (13)$$

where  $\cos \varphi = x$  is the angle cosine between relative  $\mathbf{v}_{pb}$  and center of mass  $\mathbf{V}_c$  velocities and  $m_{pb} = m_p m_b / (m_p + m_b)$  is the reduced mass of projectile and background particles. Since the scattering in the C.M. frame is axially symmetric about the relative speed  $\mathbf{v}_{pb}$ , transverse components average is zero in the scattering process, so the second term on the right of this equation will be removed.

Since there is a unit Jacobian ( $j(\mathbf{v}_p, \mathbf{v}_b; \mathbf{V}_c, \mathbf{v}_{pb}) = 1$ ) in passing to center of mass coordinate  $d\mathbf{v}_p d\mathbf{v}_b = j(\mathbf{v}_p, \mathbf{v}_b; \mathbf{V}_c, \mathbf{v}_{pb}) d\mathbf{V}_c d\mathbf{v}_{pb}$ , by replacing the Eqs. (6) and (13) into Eq. (7) and changing variables, we have,

$$\begin{aligned} \frac{d\varepsilon_{pb}^B}{dt} &= \frac{n_p n_b m_p m_b^{3/2} \sqrt{2\alpha}}{\Delta T_b^{3/2}} \int_0^\infty dV_c \int_0^\infty dv_{pb} \int_{-1}^1 x dx \left( V_c^2 + \frac{m_b^2 v_{pb}^2}{M_{pb}^2} + \frac{2m_b v_{pb} V_c x}{M_{pb}} \right)^{-1/2} \times \\ &\exp \left\{ -\frac{\alpha}{\Delta^2} \left[ \frac{m_p^2 V_c^4}{4} + \frac{m_{pb}^4 v_{pb}^4}{4m_p^2} + m_{pb}^2 (v_{pb} V_c x)^2 - \left( m_p T_p - \frac{\Delta^2 m_b}{2\alpha T_b} - m_{pb} m_p v_{pb} V_c x \right) V_c^2 \right] \right\} \end{aligned}$$

$$I_1(E_c), \quad \left. - \left( \frac{T_p}{m_p} - \frac{\Delta^2}{2m_b\alpha T_b} - \frac{m_{pb}}{m_p} v_{pb} V_c x - \frac{V_c^2}{2} \right) m_{pb}^2 v_{pb}^2 - \left( 2T_p + \frac{\Delta^2}{\alpha T_b} \right) m_{pb} v_{pb} V_c x + T_p^2 \right\} \quad (14)$$

where  $M_{pb} = m_p + m_b$  is the total mass and the integral  $I_1(E_c)$  is defined as,

$$I_1(E_c) = \int_{\mu_{min}}^1 \left( \frac{d\sigma_{pb}}{d\Omega} \right) (\mu - 1) d\mu, \quad (15)$$

In quantum mechanics between the particle that scatters at an angle  $\Theta$  from the one that scatters at  $(\pi - \Theta)$  for identical particles are not distinguishable. As a result,  $\mu_{min}$  is zero for identical particles and it is one for distinguishable particles. The integral  $I_1(E_c)$  is calculated by extracting experimental data for elastic scattering cross sections. The results are shown in Fig. (1) for D+D, and in Fig. (2) for D+T scattering, respectively.

Changing variable  $v_{pb}$  to the total kinetic energy of particles at the center of mass system  $E_c = \frac{1}{2} m_{pb} v_{pb}^2$ , the Eq. (14) may be written as the simple form,

$$\frac{d\varepsilon_{pb}^B}{dt} = \frac{4n_p n_b m_p m_b^{3/2} \sqrt{\alpha}}{\Delta m_{pb}^{3/2} T_b^{3/2}} \int_0^\infty dE_c E_c^{3/2} I_1(E_c) \int_0^\infty dV_c V_c^3 I_2(E_c, V_c), \quad (16)$$

where the integral  $I_2(E_c)$  is defined as,

$$I_2(E_c, V_c) = \int_{-1}^1 dx x \left( V_c^2 + \frac{2E_c}{m_p^2} + \frac{V_c x (8E_c m_{pb})^{1/2}}{m_p} \right)^{-1/2} \exp(-ax^2 + bx + c) \quad (17)$$

where the coefficients are,

$$\begin{cases} a = \frac{2\alpha}{\Delta^2} m_{pb} V_c^2 E_c \\ b = \frac{\alpha}{\Delta^2} \left( 2T_p + \frac{\Delta^2}{\alpha T_b} - m_p V_c^2 - \frac{2E_c m_{pb}}{m_p} \right) V_c (2E_c m_{pb})^{1/2} \\ c = \frac{\alpha}{\Delta^2} \left( m_p T_p V_c^2 + \frac{2E_c m_{pb} T_p}{m_p} - T_p^2 - \frac{m_{pb}^2 E_c^2}{m_p^2} - m_{pb} V_c^2 E_c \right) - \frac{m_b V_c^2}{2T_b} - \frac{m_{pb} E_c}{T_b m_b}, \end{cases} \quad (18)$$

The temperature equilibration rate due to binary collisions (Eq.(16)) versus temperature difference  $\Delta T = T_p - T_b$  between projectile and background particles for background temperatures  $T_b=1$  keV, 10 keV and 100 keV are depicted in Figs. (3), (4) and (5), respectively. The highest projectile temperature is chosen  $T_D=10$  MeV and the background



density is taken  $\rho_b = 300 \text{ gcm}^{-3}$ . In these figures, the ions and electron contributions denoted by the dashed and dotted lines, respectively, and the solid line represents the sum of ions and electron contributions. The results predicate that for lower background temperature ( $T_b=1 \text{ keV}$ ), the contribution of electron is dominant (Fig. (3)). By increasing the background temperature, the contribution of ions increases (Fig. (4)), specially for  $\Delta T \leq 1.5 \text{ MeV}$  it is predominant due to Bragg peak [21]. In Fig. (5) it can be seen that for  $T_b=100 \text{ keV}$  the contribution of ions is dominant over the entire range of temperature difference.

## 4 The Energy Exchange Rate Due to Collective Interactions

The Lenard-Balescu equation for the case of interest in which each background plasma species  $b$  is in thermal equilibrium by itself, is described by a Maxwell-Boltzmann distribution function (Eq. (3)) [22],

$$\frac{d\varepsilon_{pb}^{\text{LB}}}{dt} = \int \frac{d^3p_p}{(2\pi\hbar)^3} \frac{p_p^2}{2m_p} \nabla_{\mathbf{p}_b} \cdot \mathbf{L}_{pb}, \quad (19)$$

where  $\mathbf{L}_{pb}$  is the Lenard-Balescu Kernel,

$$\mathbf{L}_{pb} = \int \frac{d^3k}{(2\pi)^3} \pi \mathbf{k} \left| \frac{4\pi Z_p e Z_b e}{k^2 \varepsilon(k, v_p, \mathbf{k})} \right|^2 I_{pb}^{\text{LB}}(v_p), \quad (20)$$

In Eq. (20),  $\varepsilon(k, v_p, \mathbf{k})$  is the dielectric function that is given by [23].

$$\varepsilon(\mathbf{k}, \omega) = 1 + \sum_c \frac{4\pi(Z_c e)^2}{k^2} \int \frac{d^3p_c}{(2\pi\hbar)^3} \frac{1}{\omega - \mathbf{k} \cdot \mathbf{v}_c + i\eta} \mathbf{k} \cdot \nabla_{p_c} f_c(\mathbf{p}_c), \quad (21)$$

where the prescription  $\eta \rightarrow 0^+$  is implicit and defines the correct retarded response. The structure of the dielectric function can be simplified as,

$$k^2 \varepsilon(\mathbf{k}, \omega) = k^2 + F(\omega), \quad (22)$$

where

$$F(\omega) = F_p(\omega) + F_b(\omega), \quad (23)$$

The F functions appear in the form of a dispersion relation,

$$\begin{cases} F_p(\omega) = -4\pi(Z_p e)^2 \int \frac{d^3 p_p}{(2\pi\hbar)^3} f_p(\mathbf{p}_p) \left\{ \frac{1}{p_p^2} + \frac{2\alpha}{\Delta m_p} \left( \frac{p_p^2}{2\Delta m_p} - \frac{E_0}{\Delta} \right) \right\} \frac{\mathbf{k} \cdot \mathbf{p}_p}{\omega - \mathbf{k} \cdot \mathbf{v}_p + i\eta} \\ F_b(\omega) = -\sum_b \frac{4\pi(Z_b e)^2 \beta_b}{m_b} \int \frac{d^3 p_b}{(2\pi\hbar)^3} f_b(\mathbf{p}_b) \frac{\mathbf{k} \cdot \mathbf{p}_b}{\omega - \mathbf{k} \cdot \mathbf{v}_b + i\eta}, \end{cases} \quad (24)$$

These functions can be written as dispersion relations,

$$\begin{cases} F_p(\omega) = -\int_0^\infty dv \frac{\rho_p(v)}{\frac{\omega}{k} - v + i\eta} \\ F_b(\omega) = -\int_{-\infty}^\infty dv \frac{\rho_{total}(v)}{\frac{\omega}{k} - v + i\eta}, \end{cases} \quad (25)$$

with the spectral weight,

$$\begin{cases} \rho_p(v) = \frac{k_p^2 \sqrt{\alpha}}{2\beta_p \Delta} \left\{ \frac{1}{v} + \frac{2\alpha m_p v}{\Delta} \left( \frac{m_p v^2}{2\Delta} - \frac{E_0}{\Delta} \right) \right\} \exp \left\{ -\alpha \left( \frac{m_p v^2}{2\Delta} - \frac{E_0}{\Delta} \right)^2 \right\} \\ \rho_{total}(v) = \sum_b \rho_b(v), \end{cases} \quad (26)$$

where  $\rho_b(v)$  is the contribution of species b to the total spectral weight,

$$\rho_b(v) = k_b^2 v \sqrt{\frac{\beta_b m_b}{2\pi}} \exp \left\{ -\frac{1}{2} \beta_b m_b v^2 \right\} \quad (27)$$

and  $k_c^2$  is the contribution of c particle with charge  $Z_c e$  to the squared Debye wave number

$$k_c^2 = 4\pi\beta_c Z_c^2 e^2 n_c, \quad (28)$$

The integral  $I_{pb}^{LB}(v_p)$  in Eq. (20) is obtained as,

$$I_{pb}^{LB}(v_p) = \int \frac{d^3 p_p}{(2\pi\hbar)^3} \delta(\mathbf{k} \cdot \mathbf{v}_p - \mathbf{k} \cdot \mathbf{v}_b) \mathbf{k} \cdot [\nabla_{p_b} - \nabla_{p_p}] f_p(\mathbf{p}_p) f_b(\mathbf{p}_b), \quad (29)$$

the gradient of distribution functions are,

$$\begin{cases} \nabla_{p_p} f_p(\mathbf{p}_p) = -\left\{ \frac{1}{p_p^2} + \frac{2\alpha}{\Delta m_p} \left( \frac{p_p^2}{2\Delta m_p} - \frac{E_0}{\Delta} \right) \right\} \mathbf{p}_p f_p(\mathbf{p}_p) \\ \nabla_{p_b} f_b(\mathbf{p}_b) = -\frac{\beta_b}{m_b} \mathbf{p}_b f_b(\mathbf{p}_b), \end{cases} \quad (30)$$

replacing in Eq. (29) yield,

$$I_{pb}^{\text{LB}}(\mathbf{v}_p) = \int \frac{d^3 p_p}{(2\pi\hbar)^3} \delta(\mathbf{k} \cdot \mathbf{v}_p - \mathbf{k} \cdot \mathbf{v}_b) \mathbf{k} \cdot \left\{ \frac{\beta_b \mathbf{p}_b}{m_b} + \mathbf{p}_p \left[ \frac{1}{p_p^2} + \frac{2\alpha}{\Delta m_p} \left( \frac{p_p^2}{2\Delta m_p} - \frac{E_0}{\Delta} \right) \right] \right\} f_p(\mathbf{p}_p) f_b(\mathbf{p}_b), \quad (31)$$

by separating the parallel and vertical elements of velocities with  $k$ , and delta function properties, we have,

$$\begin{cases} \delta(\mathbf{k} \cdot \mathbf{v}_p - \mathbf{k} \cdot \mathbf{v}_b) = \delta(k [v_{p\parallel} - v_{b\parallel}]) = \frac{1}{k} \delta(v_{p\parallel} - v_{b\parallel}) = \frac{1}{k} \delta(v_{b\parallel} - v_{p\parallel}) \\ \int dv_{b\parallel} \delta(v_{b\parallel} - v_{p\parallel}) f(v_{b\parallel}) = f(v_{p\parallel}), \end{cases} \quad (32)$$

the integral Eq. (31) is obtained as,

$$I_{pb}^{\text{LB}}(\mathbf{v}_p) = -\frac{\rho_b(v_{p\parallel})}{4\pi\beta_b Z_b^2 e^2} \left\{ \beta_b - m_p \left[ \frac{1}{p_p^2} + \frac{2\alpha}{\Delta m_p} \left( \frac{p_p^2}{2\Delta m_p} - \frac{E_0}{\Delta} \right) \right] \right\} f_p(\mathbf{p}_p), \quad (33)$$

By using the divergence relation,

$$\frac{p_p^2}{2m_p} \nabla_{\mathbf{p}_p} \cdot \mathbf{L}_{pb} = \nabla_{\mathbf{p}_p} \cdot \left( \frac{p_p^2}{2m_p} \mathbf{L}_{pb} \right) - \mathbf{L}_{pb} \cdot \nabla_{\mathbf{p}_p} \left( \frac{p_p^2}{2m_p} \right), \quad (34)$$

and the gradient of kinetic energy of projectile,

$$\nabla_{\mathbf{p}_p} \left( \frac{p_p^2}{2m_p} \right) = \frac{\mathbf{p}_p}{m_p} = \mathbf{v}_p, \quad (35)$$

the Eq. (19) changes as,

$$\frac{d\varepsilon_{pb}^{\text{LB}}}{dt} = \int \frac{d^3 p_p}{(2\pi\hbar)^3} \nabla_{\mathbf{p}_b} \cdot \left( \frac{p_p^2}{2m_p} \mathbf{L}_{pb} \right) - \int \frac{d^3 p_p}{(2\pi\hbar)^3} \mathbf{L}_{pb} \cdot \mathbf{v}_p = - \int \frac{d^3 p_p}{(2\pi\hbar)^3} \mathbf{L}_{pb} \cdot \mathbf{v}_p, \quad (36)$$

putting the Eqs. (20) and (33) in this equation yields,

$$\begin{aligned} \frac{d\varepsilon_{pb}^{\text{LB}}}{dt} &= \int \frac{d^3 p_p}{(2\pi\hbar)^3} \int \frac{d^3 k}{(2\pi)^3} \pi \mathbf{k} \cdot \mathbf{v}_p \left| \frac{4\pi Z_p e Z_b e}{k^2 \varepsilon(k, v_p, \mathbf{k})} \right|^2 \\ &\quad \times \frac{\rho_b(v_{p\parallel})}{4\pi\beta_b Z_b^2 e^2} \left\{ \beta_b - m_p \left[ \frac{1}{p_p^2} + \frac{2\alpha}{\Delta m_p} \left( \frac{p_p^2}{2\Delta m_p} - \frac{E_0}{\Delta} \right) \right] \right\} f_p(\mathbf{p}_p), \end{aligned} \quad (37)$$

separating the parallel and vertical elements of velocities with  $k$  and Eq. (22), with a little calculation the temperature equilibration rate is obtained as,

$$\begin{aligned} \frac{d\varepsilon_{pb}^{\text{LB}}}{dt} &= \frac{n_p \alpha^{1/2} Z_p^2 e^2}{\Delta m_p \pi^{1/2} \beta_b} \int_0^\infty \frac{dk k^3}{|k^2 + F(kp_p/m_p)|^2} \int_0^\infty dp_p (p_p/m_p) \rho_b(p_p/m_p) \\ &\times \left\{ p_p \beta_b - m_p \left[ \frac{1}{p_p} + \frac{2\alpha p_p}{\Delta m_p} \left( \frac{p_p^2}{2\Delta m_p} - \frac{E_0}{\Delta} \right) \right] \right\} \exp \left\{ -\alpha \left( \frac{p_p^2}{2\Delta m_p} - \frac{E_0}{\Delta} \right)^2 \right\}, \end{aligned} \quad (38)$$

For shorthand, this equation is written as,

$$\frac{d\varepsilon_{pb}^{\text{LB}}}{dt} = \frac{n_p \alpha^{1/2} Z_p^2 e^2}{\Delta m_p \pi^{1/2} \beta_b} \int_0^\infty dp_p G(p_p) Q(p_p) (p_p/m_p) \rho_b(p_p/m_p), \quad (39)$$

where the function  $Q(p_p)$  is,

$$Q(p_p) = \left\{ p_p \beta_b - m_p \left[ \frac{1}{p_p} + \frac{2\alpha p_p}{\Delta m_p} \left( \frac{p_p^2}{2\Delta m_p} - \frac{E_0}{\Delta} \right) \right] \right\} \exp \left\{ -\alpha \left( \frac{p_p^2}{2\Delta m_p} - \frac{E_0}{\Delta} \right)^2 \right\}, \quad (40)$$

and the function  $G(p_p)$  is defined and solved as,

$$\begin{aligned} G(p_p) &= \int_0^\infty \frac{dk k^3}{|k^2 + F(kp_p/m_p)|^2} = \\ &= \frac{y(kp_p/m_p) \ln [x^2(kp_p/m_p) + y^2(kp_p/m_p)] + x(kp_p/m_p) \arctan \left[ \frac{y(kp_p/m_p)}{x(kp_p/m_p)} \right]}{-4y(kp_p/m_p)}, \end{aligned} \quad (41)$$

where  $x(\omega)$  and  $y(\omega)$  are the real and imaginary of  $F(\omega)$  function,

$$\begin{cases} x(\omega) = \Re[F(\omega)] \\ y(\omega) = \Im[F(\omega)], \end{cases} \quad (42)$$

The results of solving Eq. (39) are drawn in Figs. (6), (7) and (8) for background temperatures  $T_b=1$  keV, 10 keV and 100 keV, respectively. The ions and electron contributions are denoted by the dashed and dotted lines, respectively, and the solid line represents the sum of ions and electron contributions. In general, the results show that the contribution of ions increases for higher background temperatures.

## 5 Total Temperature Equilibration Rate

The total temperature equilibration rate is obtained by adding contributions of the binary collisions (Eq. (16)) and collective interactions (Eq. (39)) as,

$$\frac{d\varepsilon_{pb}}{dt} = \frac{d\varepsilon_{pb}^B}{dt} + \frac{d\varepsilon_{pb}^{LB}}{dt}, \quad (43)$$

The temperature equilibration rate (Eq. (43)) of quasi-monoenergetic deuteron beam with an equimolar deuterium-tritium plasma versus temperature difference  $\Delta T$  between projectile and background particles, for background temperatures  $T_b=1$  keV, 10 keV and 100 keV are depicted in Figs. (9), (10) and (11), respectively. The highest projectile temperature is chosen  $T_D=10$  MeV and the background density is taken  $\rho_b = 300 \text{ gcm}^{-3}$ . In these figures, the contributions of the binary collisions and the collective interactions are denoted by the dashed and dotted lines, respectively, and the solid line represents the total temperature equilibration rate. The results predicate reduction of the total temperature equilibration rate by increasing the background temperature, generally. Furthermore, independent of background temperature, the temperature equilibration rate due to binary collisions has greater contribution than collective interactions. In Fig. (9) ( $T_b=1$  keV), the Bragg peak is not visible because the electron contribution dominates for fewer background temperatures. In contrast, for greater background temperatures (Figs. (10 and (11)) the Bragg peak which is quite obvious at the lower temperature differences, is a property of Coulomb collisions between ions. Also, at the higher temperature differences, temperature equilibration rate increases due to the electron contribution and nuclear elastic scattering in the binary collisions.

## 6 Conclusion

The thermal equilibrium between charged particles is crucial to understand the overall energy balance in a fusion plasma, where the ignition and burn of the plasma are strongly temperature dependent. Since quasi-monoenergetic beams are appropriate choices for ignitor in fast ignition, we calculate their temperature equilibration rate in the fusion plasma. According to the obtained results, the temperature equilibration rate increases highly by increasing projectile and background particles temperature difference,  $\Delta T$ , for high background particles temperature. In such condition, the major contribution of exchange of energy is related to the binary collisions between projectile ions and background electrons. Increasing the background temperature, the energy exchange rate is reduced gradually. In this case, the major contribution of exchange of energy is related to the interactions between the projectile and the background ions. Figs. (9, 10 and 11) show that, at low as well as high temperatures of the fuel, ( $T_b=1$  keV, 10 keV and 100 keV), the contribution of collective interactions is lower than the contribution of binary collisions in the energy exchange rate.

## References

- [1] J. D. Lindl *Inertial confinement Fusion* (Springer-Verlag, New York, (1998))
- [2] S. Atzeni and J. Meyer-ter-Vehn *The Physics of Inertial Fusion* (Oxford: Oxford University Press, (2004)).
- [3] A. Piel *Plasma Physics: An Introduction to Laboratory, Space, and Fusion Plasmas*, Springer Berlin Heidelberg, (2010).
- [4] W. M. Stacey *Fusion Plasma Physics*, John Wiley and Sons (2012).

- [5] J. P. Freidberg *Plasma Physics and Fusion Energy*, Cambridge University Press, (2008).
- [6] M. Mahdavi, R. Azadifar, and T. Koohrokhi, *Advances in High Energy Physics*, Article ID 739491, (2014).
- [7] D. G. Swanson *Plasma Kinetic Theory*, CRC Press, (2008).
- [8] L. S. Brown, D. L. Preston, and R. L. Singleton, Jr., *Phys. Rep.* **410**, 237 (2005).
- [9] L. S. Brown and R. L. Singleton, *Phys. Rev. E* **76**, 066404 (2007).
- [10] B. M. Hegelich, B. J. Albright, J. Cobble, K. Flippo, S. Letzring, M. Paffett, H. Ruhl, J. Schreiber, R. K. Schulze and J. C. Fernandez, *Nature* **439**, 441-444 (2006).
- [11] S. Ter-Avetisyan, M. Schnrer, P. V. Nickles, M. Kalashnikov, E. Risse, T. Sokollik, W. Sandner, A. Andreev, and V. Tikhonchuk *Phys. Rev. Lett.* **96**, 145006 (2006).
- [12] L. Dong-Xiao, H. Wei, S. Lian-Qiang, W. Shun-Chao and G. Yu-Qiu, *Plasma Phys. Control. Fusion* **53**, 035022 (2011).
- [13] X. Yang, G. H. Miley, K. A. Flippo, and H. Hora , *Laser and Particle Beams*, **30**, 31-38 (2012).
- [14] J. J. Honrubia, J. C. Fernandez, M. Temporal, B. M. Hegelich, J. Meyer-ter-Vehn, *Phys. Plasmas*, **16**, 102701 (2009).
- [15] J. J. Honrubia, J. C. Fernandez, M. Temporal, B. M. Hegelich, J. Meyer-ter-Vehn, *Journal of Physics: Conference Series*, **244**, 022038 (2010).
- [16] E. M. Lifshitz and L. P. Pitaevskii, *Physical Kinetics*, Pergamon Press, Oxford, (1981).

- [17] M. Mahdavi, T. Koohrokhi and R. Azadifar, *Phys. Plasmas* **19**, 082707 (2012).
- [18] C. L. Dunford, Data retrieved from the Cross Section Information Storage and Retrieval System (CSISRS) data base (Feb 27,1996); available on Internet (<http://www.nndc.bnl.gov>) (EXFORC00 23001); plot produced using the code BNL 325. National Nuclear Data Center, Brookhaven National Laboratory
- [19] A. Trkov, M. Herman and D.A. Brown (ed.), ENDF-6 formats manual: Data Formats and procedures for the evaluated nuclear data file ENDF/B-VI and ENDF/B-VII, Brookhaven National Laboratory report BNL-90365-2009 Rev. **2** (2011), available at [www.nndc.bnl.gov](http://www.nndc.bnl.gov).
- [20] M. Mahdavi and T. Koohrokhi, *Phys. Rev. E* **85**, 016405 (2012).
- [21] J. A. Frenje ,P. E. Grabowski, C. K. Li, F. H. Sguin, A. B. Zylstra, M. Gatu Johnson, R. D. Petrasso, V. Yu Glebov, T. C. Sangster, *Phys Rev Lett.* **115**, 205001 (2015).
- [22] D. R. Nicholson, *Introduction to Plasma Theory*, John Wiley and Sons, New York, (1982)
- [23] G. Zwicknagel, C. Toepffer, and P.-G. Reinhard, *Phys. Rep.* **309**, 117 (1999).



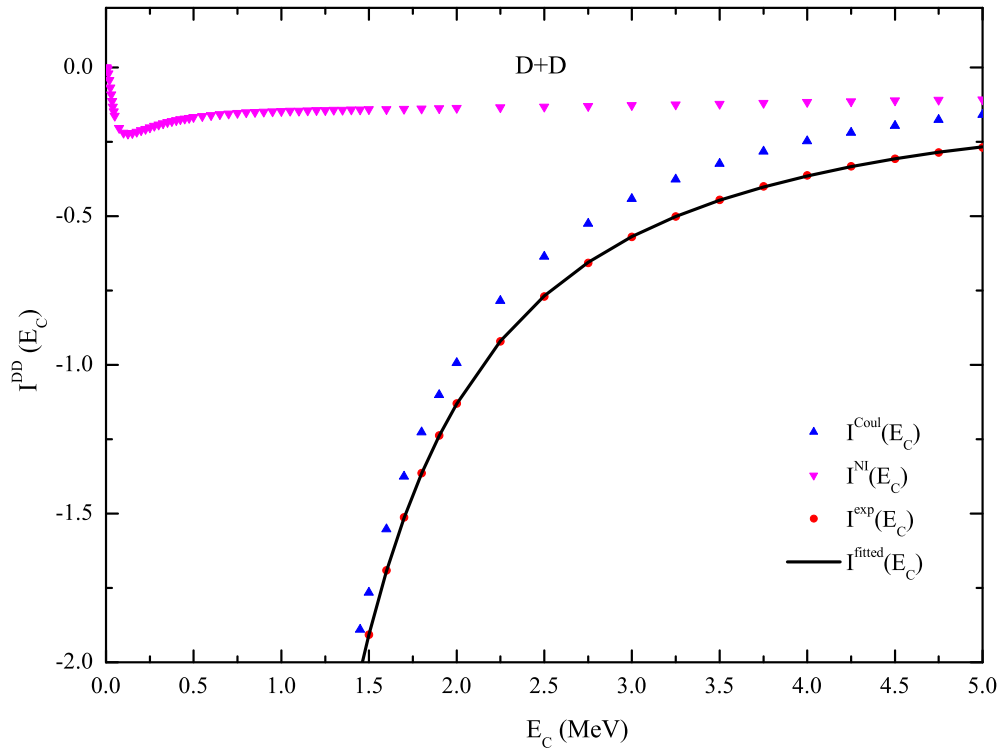


Figure 1: The integral  $I_1(E_C)$  (Eq. (15)) versus the total energy in the center of mass coordinate  $E_C$  for D+D scattering. The contributions of Coulomb, nuclear and experimental data are depicted, separately.

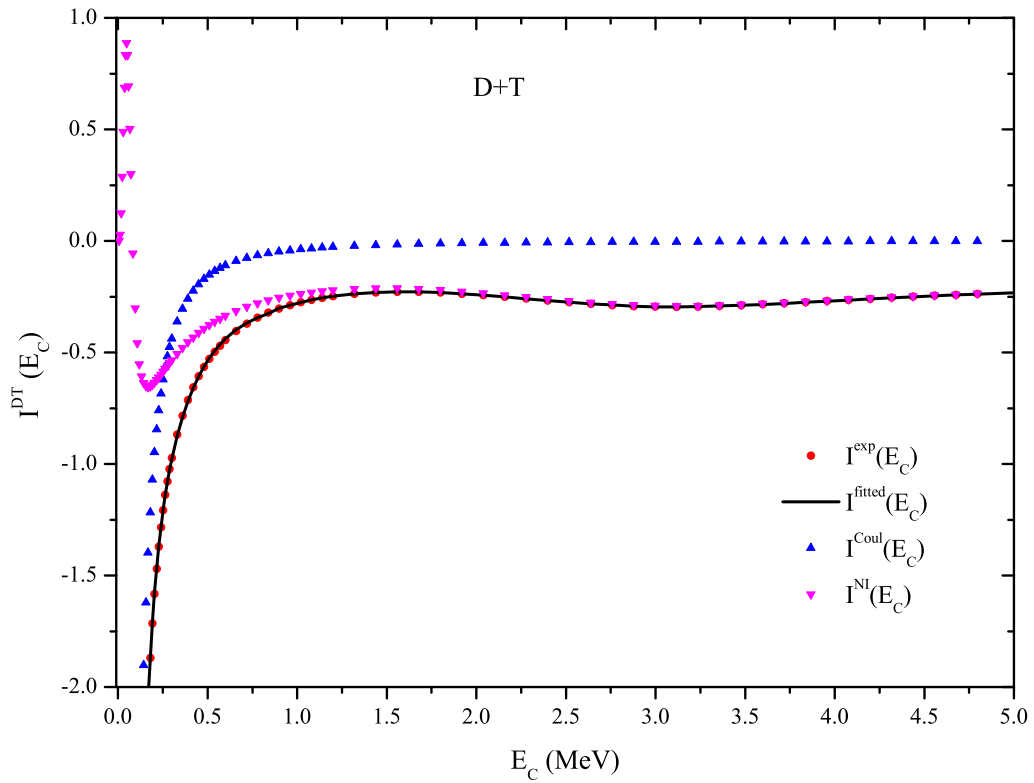


Figure 2: The integral  $I_1(E_C)$  (Eq. (15)) versus the total energy in the center of mass coordinate  $E_C$  for D+T scattering. The contributions of Coulomb, nuclear and experimental data are depicted, separately.

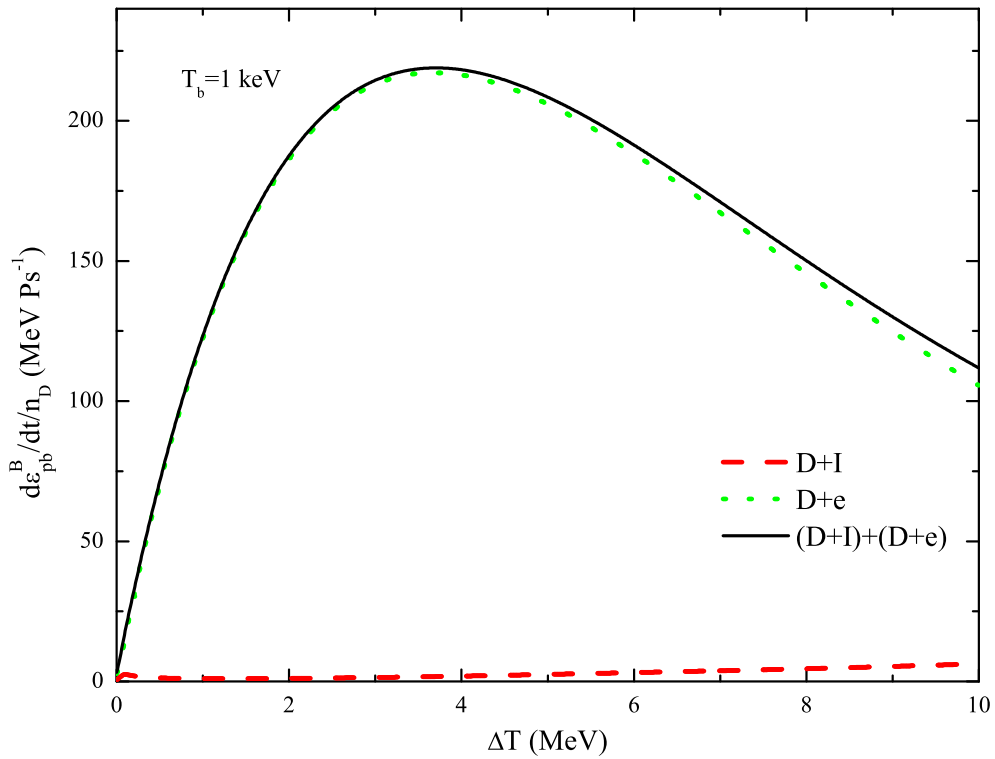


Figure 3: The temperature equilibration rate due to binary collisions (Eq.(16)) versus projectile and background particles temperature difference,  $\Delta T$ , for background temperature  $T_b=1$  keV and density  $\rho_b = 300$  gcm $^{-3}$ . The dashed and dotted lines denote ions and electron contributions, respectively and solid line is the total temperature equilibration rate.

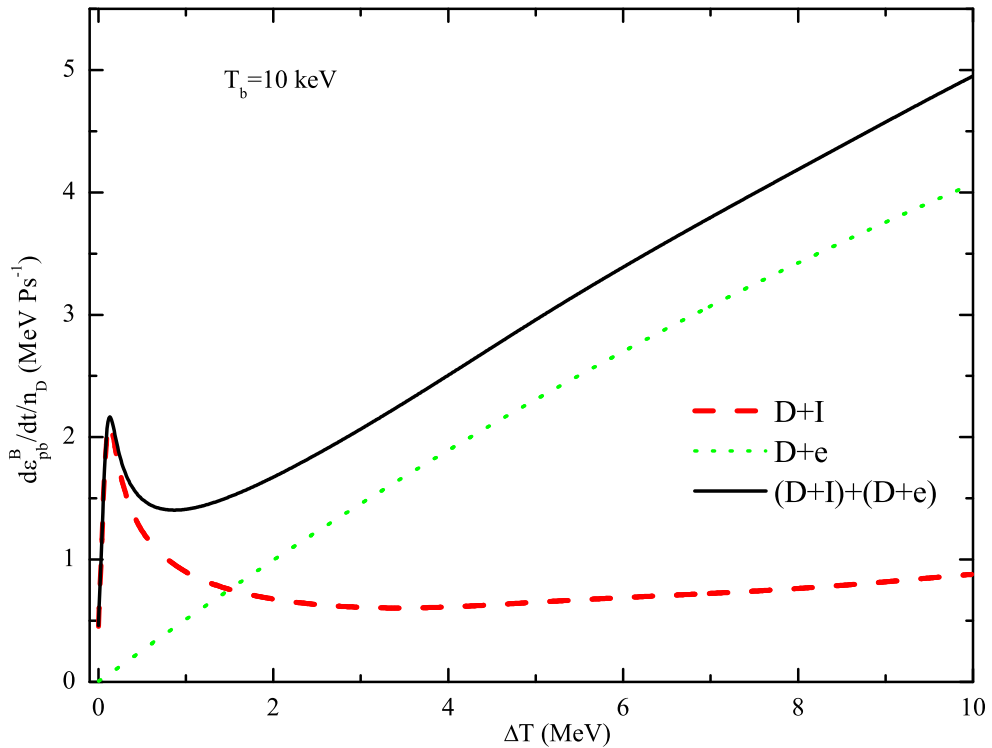


Figure 4: The temperature equilibration rate due to binary collisions (Eq.(16)) versus projectile and background particles temperature difference,  $\Delta T$ , for background temperature  $T_b=10$  keV and density  $\rho_b = 300 \text{ gcm}^{-3}$ . The dashed and dotted lines denote ions and electron contributions, respectively and solid line is the total temperature equilibration rate.

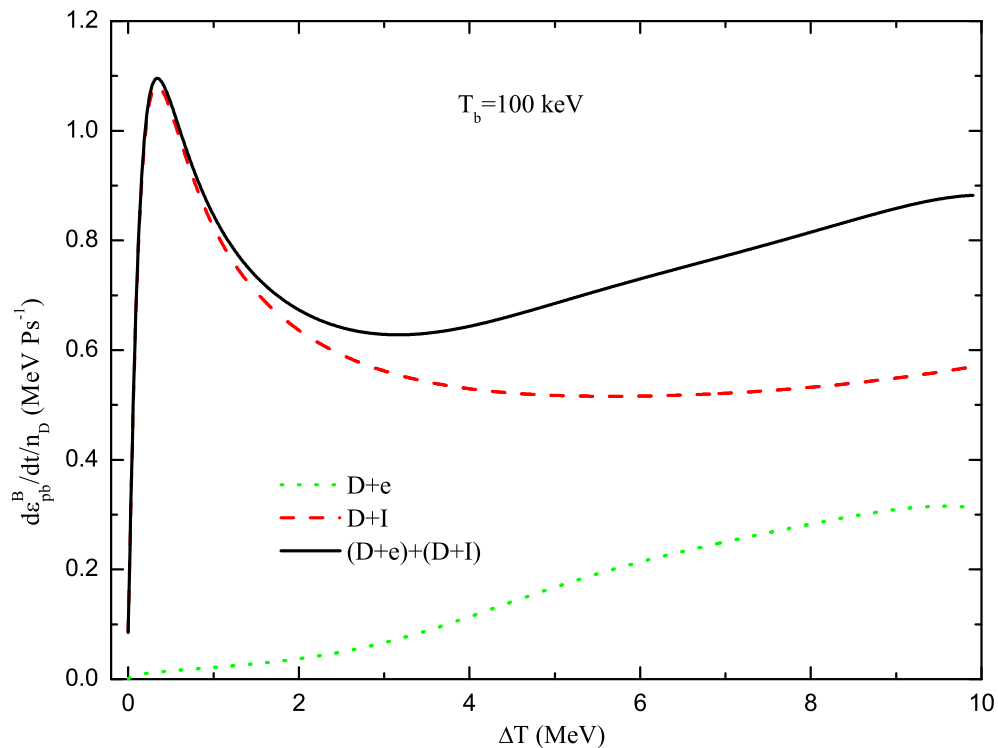


Figure 5: The temperature equilibration rate due to binary collisions (Eq.(16)) versus projectile and background particles temperature difference,  $\Delta T$ , for background temperature  $T_b=100$  keV and density  $\rho_b = 300$   $\text{gcm}^{-3}$ . The dashed and dotted lines denote ions and electron contributions, respectively and solid line is the total temperature equilibration rate.

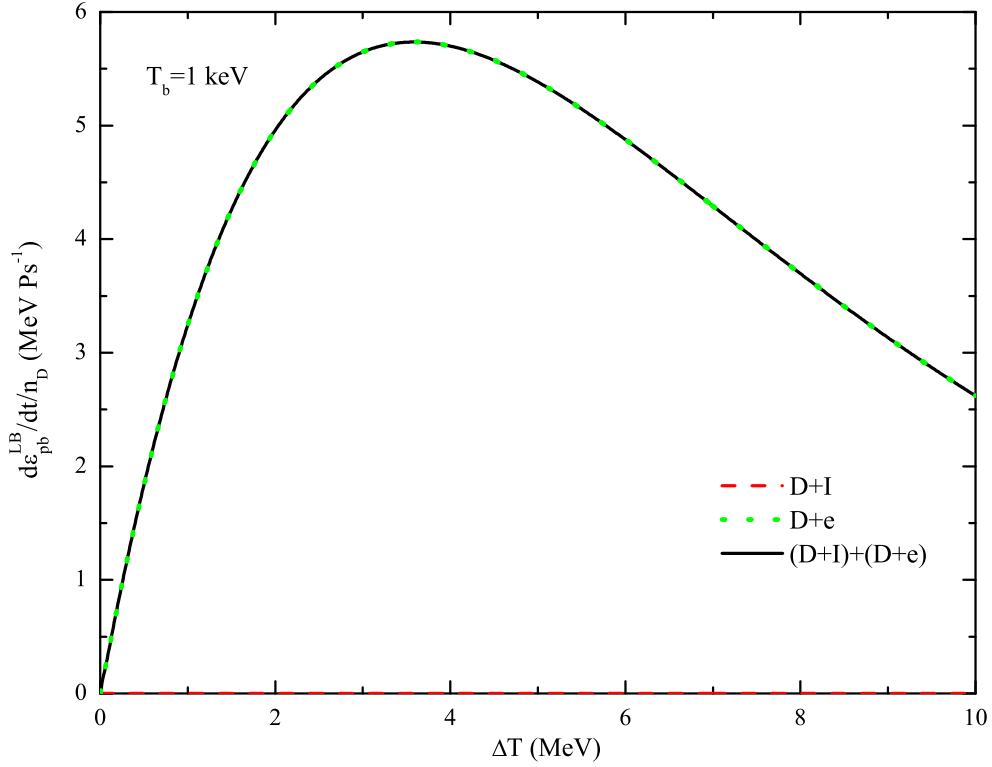


Figure 6: The temperature equilibration rate due to collective interactions (Eq.(39)) versus projectile and background particles temperature difference,  $\Delta T$ , for background temperature  $T_b=1$  keV and density  $\rho_b = 300$  gcm $^{-3}$ . The dashed and dotted lines denote ions and electron contributions, respectively and solid line is the total temperature equilibration rate.

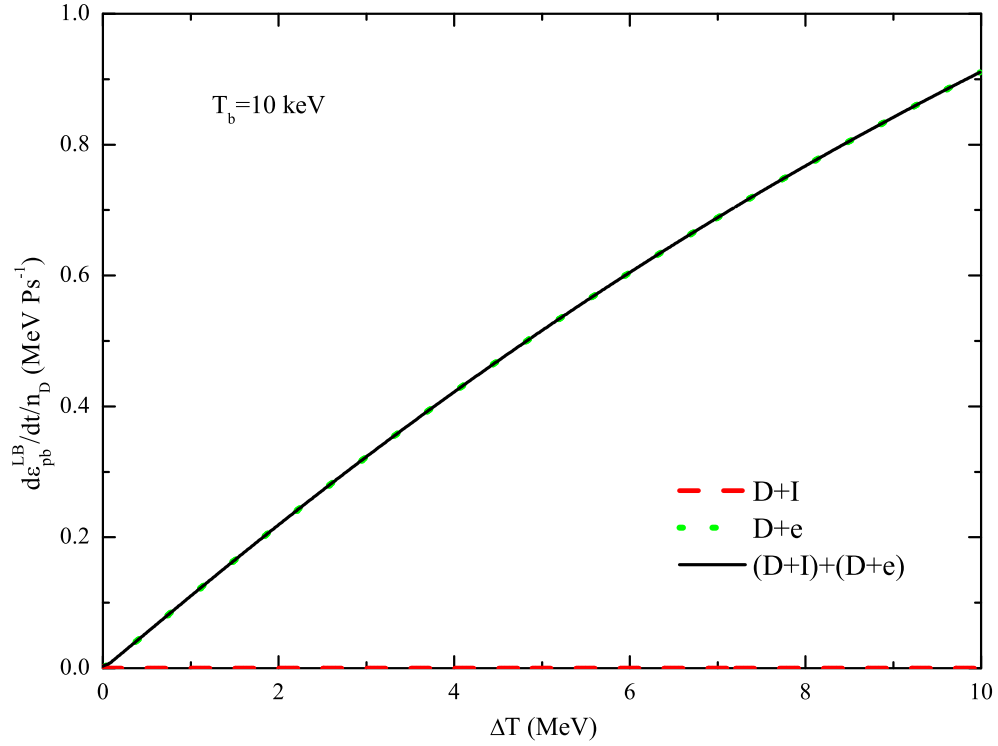


Figure 7: The temperature equilibration rate due to collective interactions (Eq.(39)) versus projectile and background particles temperature difference,  $\Delta T$ , for background temperature  $T_b=10$  keV and density  $\rho_b = 300$  gcm $^{-3}$ . The dashed and dotted lines denote ions and electron contributions, respectively and solid line is the total temperature equilibration rate.

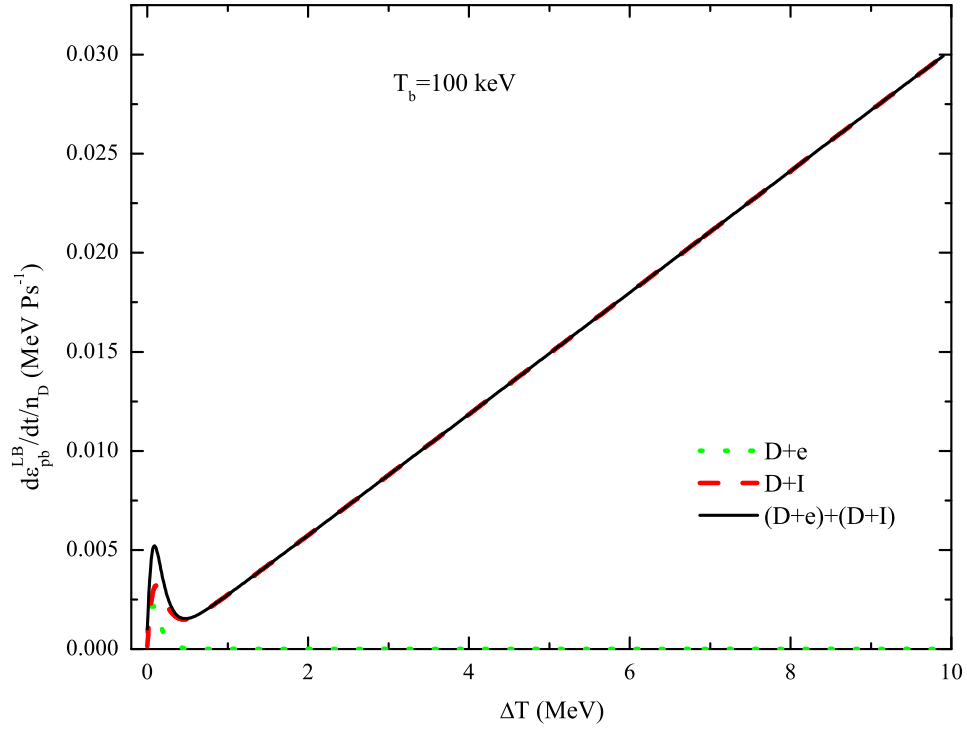


Figure 8: The temperature equilibration rate due to collective interactions (Eq.(39)) versus projectile and background particles temperature difference,  $\Delta T$ , for background temperature  $T_b=100$  keV and density  $\rho_b = 300$  gcm<sup>-3</sup>. The dashed and dotted lines denote ions and electron contributions, respectively and solid line is the total temperature equilibration rate.



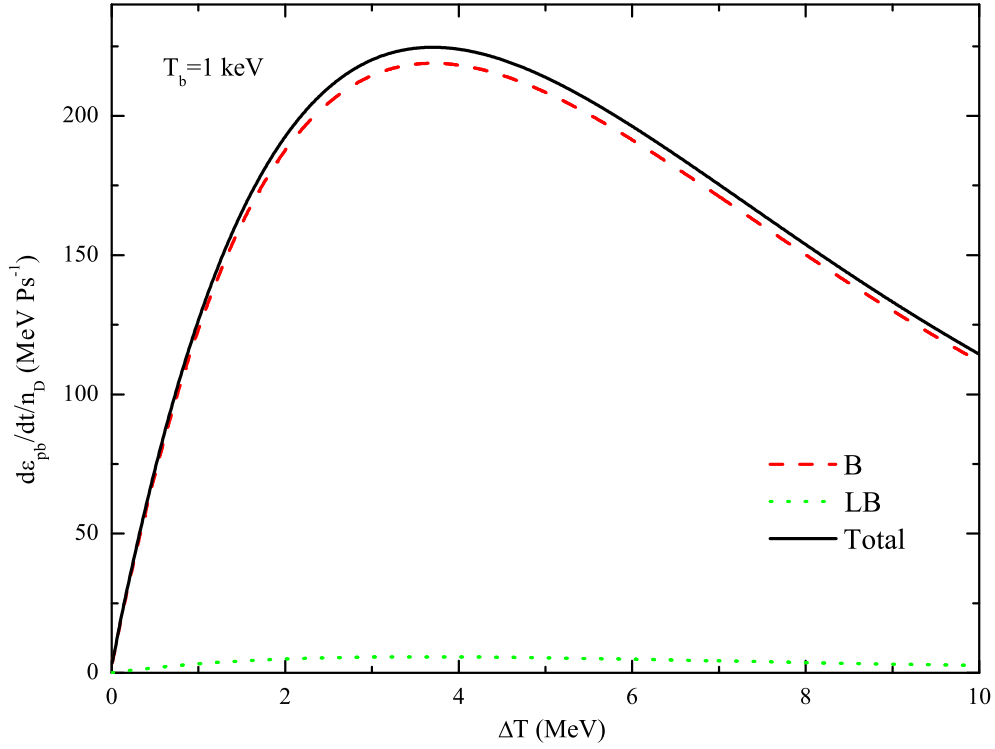


Figure 9: The temperature equilibration rate versus projectile and background particles temperature difference,  $\Delta T$ , for background temperature  $T_b=1$  keV and density  $\rho_b = 300 \text{ gcm}^{-3}$ . The dashed and dotted lines denote binary collisions (Eq. (16)) and collective interactions (Eq. (39)), respectively and solid line is the total temperature equilibration rate (Eq. (43)).

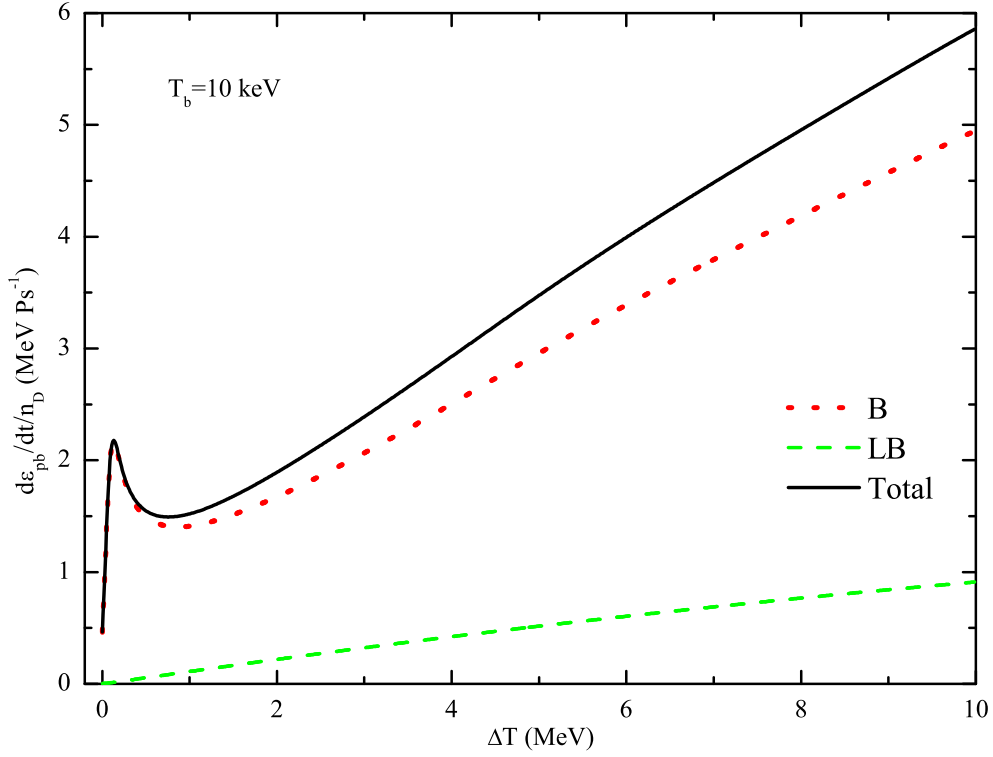


Figure 10: The temperature equilibration rate versus projectile and background particles temperature difference,  $\Delta T$ , for background temperature  $T_b=10$  keV and density  $\rho_b = 300 \text{ gcm}^{-3}$ . The dashed and dotted lines denote binary collisions (Eq. (16)) and collective interactions (Eq. (39)), respectively and solid line is the total temperature equilibration rate (Eq. (43)).

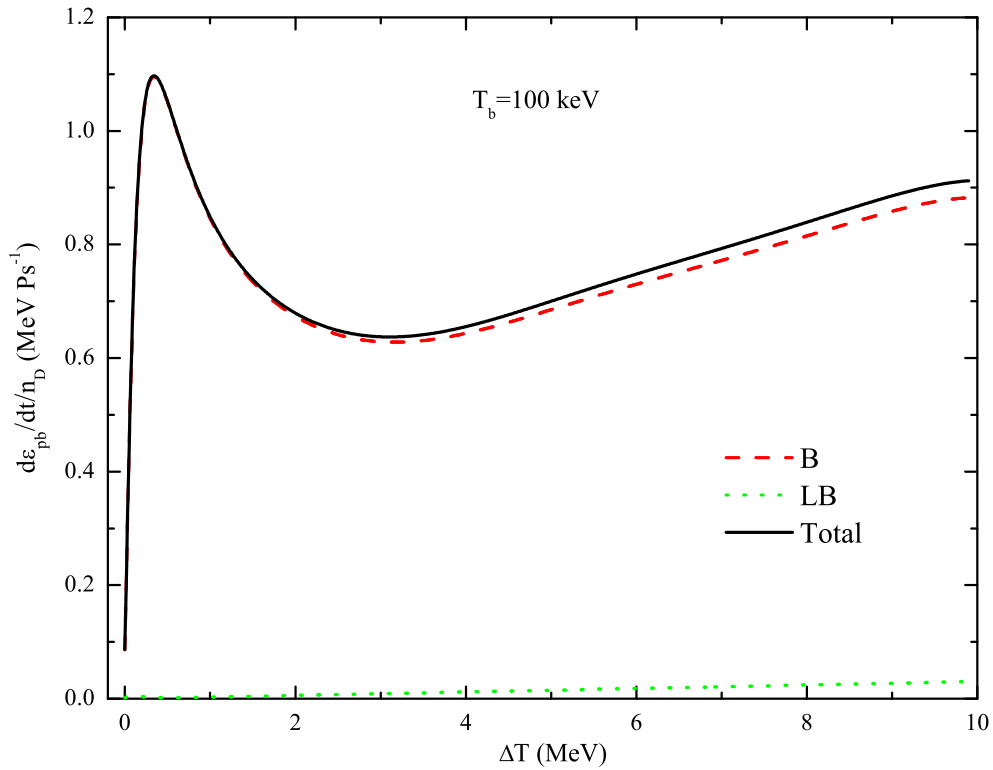


Figure 11: The temperature equilibration rate versus projectile and background particles temperature difference,  $\Delta T$ , for background temperature  $T_b=100$  keV and density  $\rho_b = 300 \text{ gcm}^{-3}$ . The dashed and dotted lines denote binary collisions (Eq. (16)) and collective interactions (Eq. (39)), respectively and solid line is the total temperature equilibration rate (Eq. (43)).